applied sciences

MDPI

Article

Development of Micro-Nano Structured Electrodes for Enhanced Reactivity: Improving Efficiency Through Nano-Bubble Generation

Kwangseok Lee [1,*], Moonsu Kim [2], Jung-Hyung Park [1], Bonggi Choi [1] and Woonbong Hwang [2]

[1] Alternative Fuels and Power System Research Center, Korea Research Institute of Ships & Ocean Engineering (KRISO), Daejeon 34103, Republic of Korea; pjhyung@kriso.re.kr (J.-H.P.); bgchoi@kriso.re.kr (B.C.)
[2] Department of Mechanical Engineering, Pohang University of Science and Technology (POSTECH), Pohang 37673, Republic of Korea; helyans@postech.ac.kr (M.K.); whwang@postech.ac.kr (W.H.)
* Correspondence: kslee@kriso.re.kr; Tel.: +82-42-866-3961

Abstract: This study focuses on developing high-performance electrodes by applying micro/nano structures to aluminum mesh electrodes and evaluating their electrochemical performance through the electroflotation process. First, the most suitable electrode material for electroflotation was selected, followed by the application of micro-nano structures to analyze bubble generation and size distribution in comparison to conventional electrodes. The bubble generation rate and size were used to predict electroflotation efficiency, which was then validated through experiments. The developed electrodes demonstrated a ninefold reduction in purification time compared to traditional electrodes and achieved higher wastewater treatment efficiency than spontaneous flotation. This research highlights the potential of micro-nano structured electrodes to enhance electroflotation processes and offers valuable insights for industrial applications.

Keywords: electroflotation; micro/nano structures; bubble generation; wastewater treatment; high-performance electrodes; separation efficiency

check for updates

Citation: Lee, K.; Kim, M.; Park, J.-H.; Choi, B.; Hwang, W. Development of Micro-Nano Structured Electrodes for Enhanced Reactivity: Improving Efficiency Through Nano-Bubble Generation. *Appl. Sci.* **2024**, *14*, 9952. https://doi.org/10.3390/app14219952

Academic Editor: Samuel Adeloju

Received: 19 September 2024
Revised: 13 October 2024
Accepted: 28 October 2024
Published: 31 October 2024

Copyright: © 2024 by the authors. Licensee MDPI, Basel, Switzerland. This article is an open access article distributed under the terms and conditions of the Creative Commons Attribution (CC BY) license (https://creativecommons.org/licenses/by/4.0/).

1. Introduction

Electrode technology is a key component in electrochemical reactions and is widely utilized across various industrial sectors. The study of electrodes began in the early 19th century with the invention of batteries [1], and over time, electrodes have become an essential component in energy storage and conversion devices. In particular, with the rapid development of green energy transition technologies in the 21st century, the importance of electrodes has become even more pronounced. Today, electrodes play a critical role not only in energy storage systems such as batteries [2–10], fuel cells [11–13], and supercapacitors [14–16], but also in hydrogen production through water electrolysis [17–21]. Both battery-based energy storage systems and water electrolysis technology are crucial in driving the transition to sustainable energy, highlighting the increasing importance of electrode technology in these fields.

Electrode technology is being researched with a focus on maximizing reaction efficiency and stability to improve performance in various applications. To optimize the reaction efficiency of electrodes, various factors must be considered, including the reaction environment [22–24], electrode materials [25–28], electrolytes [29–31], power supply conditions [32–34], and electrode modification [5–10,35,36]. Among these, electrode modification is currently dependent on techniques such as additive manufacturing [5–7] and electrodeposition [8–10], which face limitations in terms of practicality. While these methods have shown meaningful results in research settings, they may encounter challenges when scaled for industrial applications due to issues such as reduced adhesion between the electrode

substrate and additives, leading to delamination during use. This is particu-larly true when the substrate material or electrolyte composition is not adequately considered, which can exacerbate detachment under operational conditions. Additionally, these techniques often fail to adequately control surface morphology and material uniformity, potentially compromising long-term durability.

In contrast, micro- and nano-structured modifications applied directly to the electrode surface, as proposed in this study, avoid these adhesion issues by structuring the original substrate material itself [37–41]. This eliminates concerns about delamination, resulting in enhanced durability and stability over extended use. Optimizing the material structure in this way allows for simultaneous improvement in electrochemical performance and industrial practicality.

In this study, we aim to develop electrodes by applying micro- and nano-structured modifications to various metal electrodes using chemical processes. These methods have demonstrated high productivity and durability in previous research [37–41], and we plan to evaluate their electrochemical performance using the electroflotation (EF) process.

EF, as illustrated in Figure 1, is an emerging wastewater treatment technology that has garnered attention in recent years for its numerous advantages over traditional methods, such as dissolved air flotation (DAF) [42–44]. EF effectively separates solids from liquids by utilizing gases produced during water electrolysis, offering significant benefits in terms of cost efficiency, stability, and environmental protection. The fundamental efficiency of EF depends on the amount and size of gas bubbles generated per unit electrode area. Smaller and more abundant bubbles improve separation efficiency by continuously facilitating efficient contact between the electrode and the liquid, which is closely related to reactivity [35,36,45,46]. In this study, we will select industrial-grade metals suitable for bubble generation, apply micro- and nano-structures to these metals, and meticulously examine bubble size and quantity during the EF process to develop electrodes with enhanced reactivity.

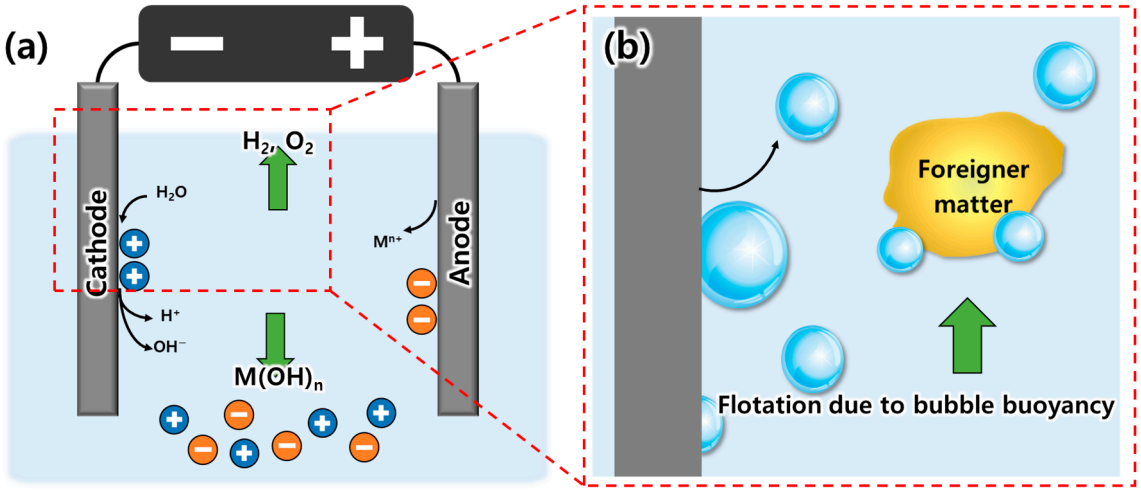

Figure 1. Schematics of (**a**) electroflotation process and (**b**) flotation mechanism.

This study focuses on analyzing the effects of electrode morphology and micro-nano structures on the EF process, investigating the mechanisms of bubble generation and size distribution, and evaluating the reactivity and overall flotation performance of the developed electrodes. The findings of this research are expected to provide valuable insights into the design and fabrication of high-performance electrodes for EF applications, contributing to the improvement of system performance where electrodes are utilized.

2. Experimental Section

2.1. Material Selection

To select the optimal electrode material for enhancing EF performance, industrial aluminum (5052, >99.5% purity), titanium (6 A l4 V, <90% purity), and copper plate (C11,000, >99.9% purity) were processed into 50 mm × 10 mm × 1 mm specimens for use in the experiments. A 3.5% electrolyte solution was prepared using sodium chloride (NaCl, 99.5%), also sourced from SAMCHUN Chemical, Pohang, Korea. The metal plate of each candidate material was connected to the anode, while a platinum plate was attached to the cathode. The electrodes were then immersed in the prepared NaCl solution and subjected to a constant voltage of 10 V. The bubble generation rate was recorded and compared for each electrode material, with each experiment repeated three times to calculate the average and standard deviation for each material.

2.2. Electrode Modification

2.2.1. Surface Treatment

For the electrode modification experiments, industrial aluminum plates and aluminum mesh electrodes of the same dimensions were utilized. The aluminum plates were supplied by Almarket, Daegu, Korea, while the aluminum mesh was sourced from TWP Inc., Berkeley, CA, USA. The mesh had an opening size of 0.28 mm, a wire diameter of 0.23 mm, and a density of 50 pores per inch (ppi). Both the aluminum plate and mesh electrodes underwent a two-step process consisting of surface etching and crystallization to introduce micro-nano structures on the material surfaces. Initially, the electrodes were etched in a 1 M hydrochloric acid (HCl, 35.0~37%) solution, sourced from SAMCHUN Chemical, Korea, at room temperature for 30 s. Following the etching process, the electrodes were immersed in a solution of 1 M sodium hydroxide (NaOH, bead, 98.0%), also sourced from SAMCHUN Chemical, Korea, at 80 °C for 10 min to facilitate crystallization. The electrodes were then dried in an 80 °C oven for 60 min.

2.2.2. Characterization of Electrode Surface Morphology and Bubble Behavior

The surface morphology of the fabricated electrodes, including the micro-nano structures, was analyzed using a high-resolution Field Emission-Scanning Electron Microscope (FE-SEM; JM-7401F, JEOL, Tokyo, Japan) to confirm the successful formation of these structures on the electrode surface. The bubble behavior for both pristine and micro-nano structured electrodes was visually observed using a high-speed camera (Y7, IDT, Passadena, CA, USA) operating at 5000 frames per second. The size and distribution of the generated fine bubbles were measured using Nano Tracking Analysis (NTA), conducted using the NanoSight NS300 instrument from Malvern Panalytical (Malvern, UK). The total volume of bubbles produced was measured by recording the amount of gas generated at the anode for 5 min, and then calculating the bubble production rate by dividing the total volume by time (in seconds). This method was used for each electrode to obtain bubble production rates.

2.3. Evaluation of EF Performance

Oil-in-water emulsions were prepared to evaluate the flotation performance of the micro-nano structured mesh electrodes for various oil types, including gasoline, diesel, naphtha (Petroleum, 95.0%), n-hexane (C_6H_{14}, >96.0%), and toluene ($C_6H_5CH_3$, 99.5%). Gasoline and diesel were supplied by HD Hyundai Oilbank, Pohang, Korea, while the other oil types were sourced from SAMCHUN Chemical, Korea. The oils were mixed with a 3.5% sodium chloride (NaCl) solution at a volume ratio of 1:9, and the mixtures were homogenized at 5000 rpm for 10 min to ensure a uniform distribution of oil droplets in the solution.

The EF experiments were performed using the modified electrodes in a custom-built electrolytic cell. Two conditions were compared to assess the degree of oil flotation and residual oil content in the solution: spontaneous flotation (Figure 2a) and 10 min electrolysis

at 100 V in a 3.5% NaCl solution (Figure 2b). The EF process was conducted using both pristine and micro-nano structured mesh electrodes to determine the impact of surface structures on the flotation performance.

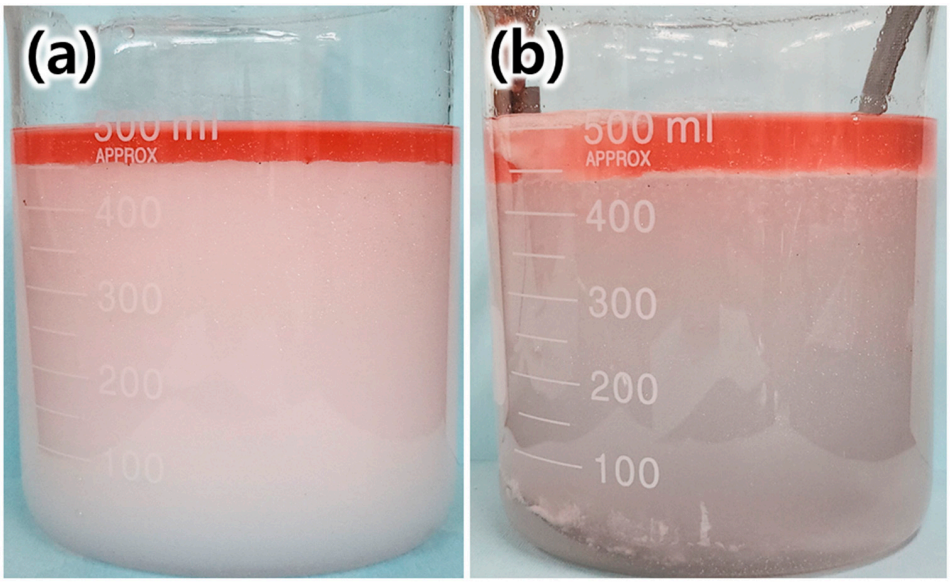

Figure 2. Photographs of the results of (**a**) spontaneous flotation and (**b**) EF of the oil-in-water mixture for 10 min.

After the EF process, the residual oil concentrations in the solution were measured using Total Organic Carbon (TOC) analysis with a Total Organic Carbon analyzer (TOC-L, Shimadzu, Japan). The results were compared to evaluate the efficiency of the micro-nano structured mesh electrodes in removing various oil types from the water.

3. Results and Discussion

3.1. Material Selection

EF, based on water electrolysis, is governed by two dominant reactions: the dissolution of metal at the anode due to oxidation and the generation of hydrogen gas at the cathode from the electrolysis of water [47]. These reactions can be described using Equations (1) and (2), respectively:

$$\mathrm{M}(s) \rightarrow \mathrm{M}^{n+}(aq) + ne^- \quad (1)$$

$$n\mathrm{H_2O} + ne^- \rightarrow \frac{1}{2}n\mathrm{H_2}(g) + n\mathrm{OH}^- \quad (2)$$

$$\mathrm{M}^{n+}(aq) + n\mathrm{OH}^- \rightarrow \mathrm{M(OH)}_n(s) \quad (3)$$

During EF, metals dissolve into the solution, forming divalent or trivalent cations depending on the solution pH and potential. Simultaneously, the generated hydroxide ions (OH^-) react with dissolved metal cations to form metal hydroxides, which precipitate as described in Equation (3). These precipitates can aggregate with other impurities, positively contributing to water purification [48].

If improper electrode materials are selected or inappropriate electrolyte concentrations and voltage/current conditions are applied, unwanted side reactions may occur. For instance, gas evolution from the electrolyte can happen at the anode, or metal precipitation can occur at the cathode. In some cases, the actual oxidation rate at the anode does not match predictions based on Faraday's law. This discrepancy can be attributed to the local

pH increase caused by continuous OH^- production or, at sufficiently high anode potentials, the occurrence of the oxygen evolution reaction, as represented by Equation (4) [43,49,50]:

$$2H_2O \rightarrow O_2 + 4H^+ + 4e^- \quad (4)$$

These reactions, including gas evolution and metal hydroxide precipitation, can be visually represented in Figure 1. Based on this theoretical understanding, an experiment was conducted to determine the most suitable electrode material for enhancing EF performance by maximizing bubble generation.

Since a higher bubble generation rate increases the likelihood of collisions between bubbles and oil droplets, leading to improved separation efficiency, it was crucial to select a material with a high bubble generation rate. To this end, we observed and compared the bubble generation rates for aluminum, titanium, and copper electrodes, as shown in Figure 3. The results indicated that aluminum electrodes exhibited the highest bubble generation rate of 19.2 mm^3/s, surpassing both titanium and copper electrodes (Figure 3d). This outcome aligns with the known ionization tendencies of the metals (Al > Ti > Cu) under constant voltage conditions [51]. Based on these observations, aluminum was selected as the most suitable electrode material for further studies aimed at optimizing EF performance.

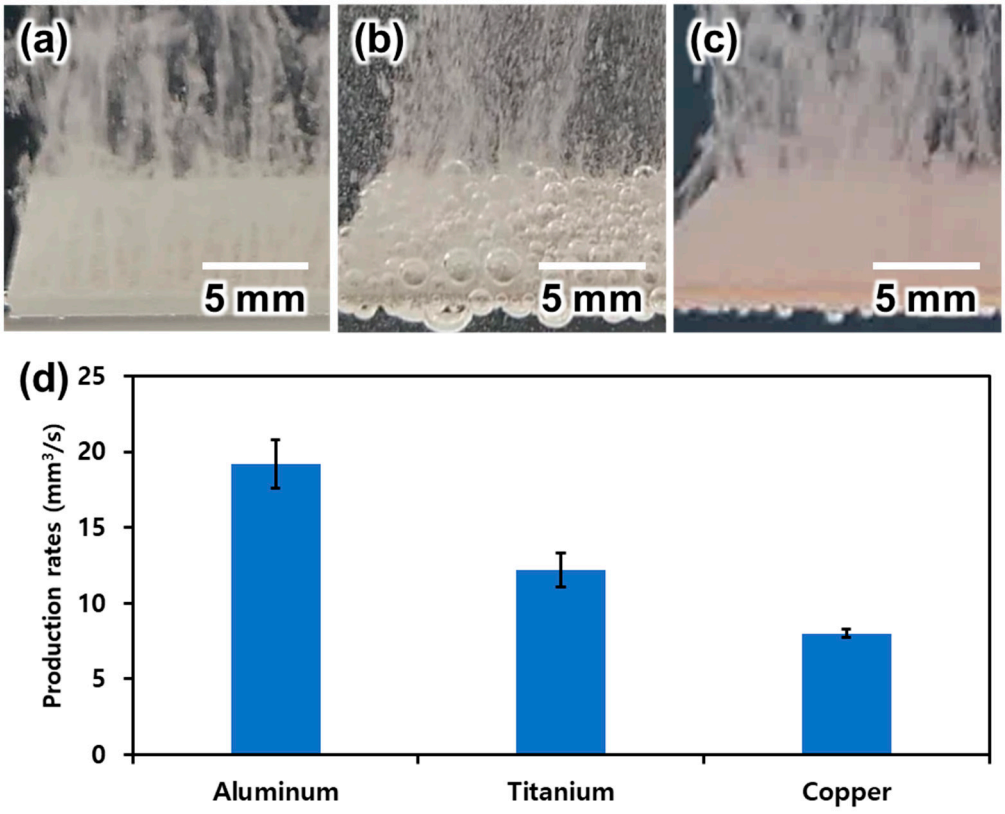

Figure 3. Bubble generation for (**a**) aluminum, (**b**) titanium, and (**c**) copper electrodes; (**d**) comparison of bubble production rates across materials.

3.2. Evaluation of Bubble Generation for Various Types of Electrodes

When reactions occur at the electrode, gas bubbles are generated at the electrode surface, as represented by Equations (2) and (4). The generated bubbles are subject to buoyancy force (F_b) and surface tension (F_σ) at the electrode, and the buoyancy force can be expressed using Equations (5) and (6) (Figure 4a,b) [52]:

$$F_b = \frac{4}{3}\pi(\rho_{liquid} - \rho_{gas})gr^3 \quad (5)$$

$$F_\sigma = p\sigma sin\theta \quad (6)$$

where ρ_{liquid} is the liquid density of the electrolyte, ρ_{gas} is the gas density, g is gravitational acceleration, and r is the radius of the bubble. p is the length of the contact line and σ is the dynamic surface tension between the bubble and the electrode surface.

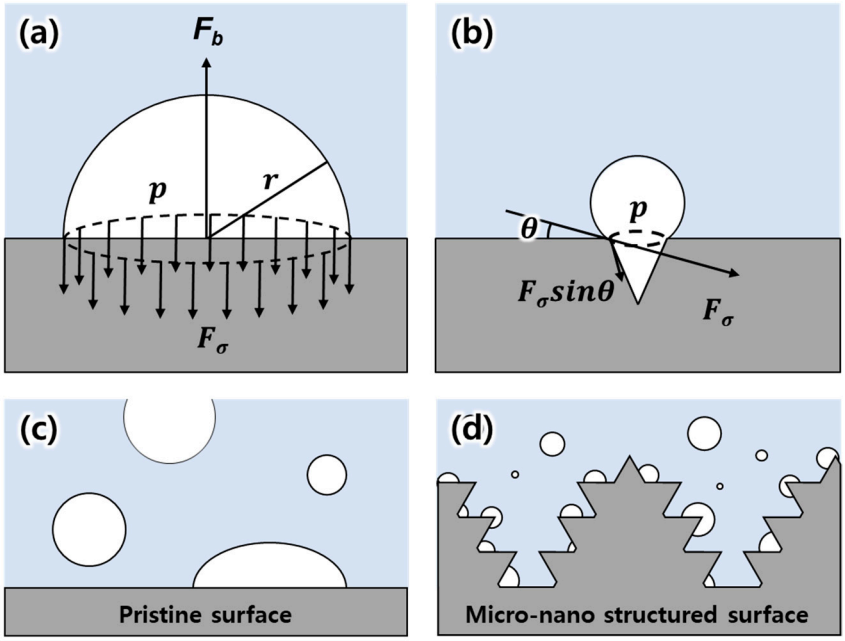

Figure 4. Schematic force diagram and generation of bubble on (**a**,**c**) pristine and (**b**,**d**) micro-nano structured surface.

When surface tension exceeds buoyancy, larger bubbles are formed, and the buoyancy force increases. Once the buoyancy force surpasses surface tension, the bubbles detach from the electrode surface into the solution. The larger bubble size observed with the titanium electrode (Figure 3) is attributed to the higher surface tension (σ) of titanium (Ti > Cu > Al) compared to other materials [53–55].

According to Equation (6), on a pristine surface, where the contact angle θ is 90°, the maximum cohesive force acts on the bubbles, resulting in the formation of larger bubbles. When bubbles form on the electrode surface, no reaction occurs in the area covered by the bubbles, which negatively affects electrode efficiency. Therefore, the generation of large bubbles can hinder the electrode's overall performance. In contrast, when micro-nano structures are present on the electrode surface, the value of θ changes, reducing the cohesive force and promoting the consistent formation of smaller bubbles. The continuous release of fine bubbles ensures that the electrolyte infiltrates the electrode surface, allowing for further reactions and enhancing the overall efficiency. Additionally, the use of micro-nano structures increases the surface area of the electrode, providing more active sites for reactions compared to a pristine surface (Figure 4c,d).

Based on this theoretical framework, we investigated the effect of surface structures on bubble size and distribution by fabricating four types of aluminum electrodes: Plate-Pristine (PP), Plate-Micro/Nano (PMN), Mesh-Pristine (MP), and Mesh-Micro/Nano (MMN). Mesh electrodes were chosen because they offer a simple method to increase surface area. The surface morphology of the fabricated electrodes was examined using Scanning Electron Microscopy (SEM) to confirm the successful formation of the micro/nano structures (Figure 5). In particular, the interfacial bonds between the micro/nano structures and substrates consist of hydrogen bonding with the hydroxyl groups, which leads to a condensation reaction and covalent bonding to the substrate. This chemical treatment ensures improved durability and stability, as demonstrated in previous studies [37–41].

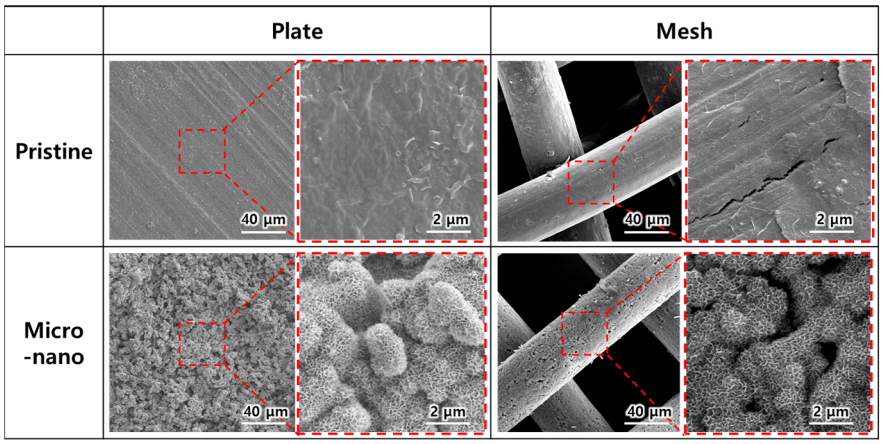

Figure 5. The SEM image of various electrode surfaces: Plate-Pristine (PP), Plate-Micro/Nano (PMN), Mesh-Pristine (MP), and Mesh-Micro/Nano (MMN).

To assess the effect of surface structures on bubble generation, the macroscopic process of bubble generation during electrolysis was observed using a high-speed camera, and the size and distribution of bubbles were evaluated using optical instruments under identical experimental conditions (Figure 6). Figure 6a,b show images of bubbles generated by the MP and MMN electrodes, respectively. In the MP electrode, large bubbles visible to the naked eye predominantly formed. In contrast, the MMN electrode exhibited very few visible bubbles, with most bubbles appearing as a mist due to their significantly smaller size. The macroscopic process of bubble generation can be viewed in Supplementary Materials Videos S1 and S2.

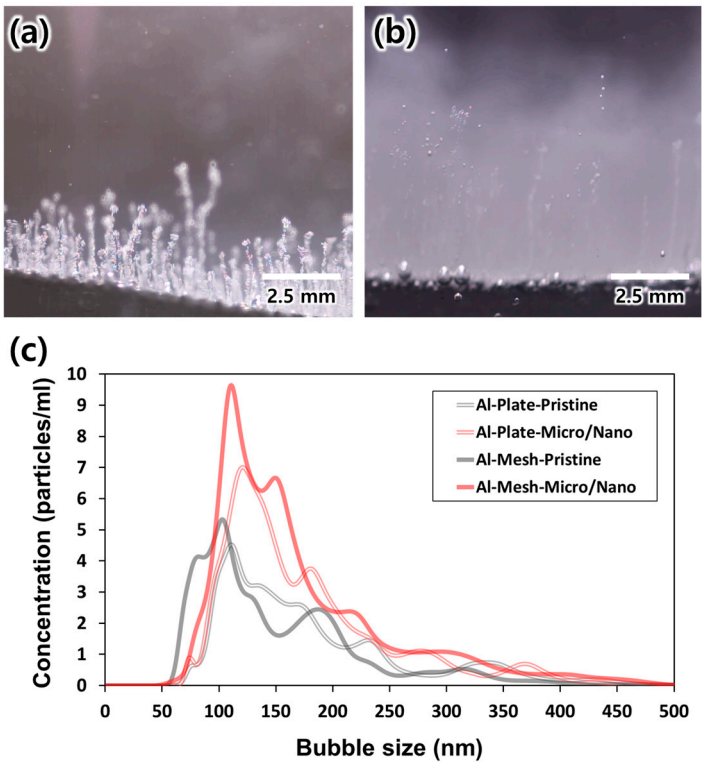

Figure 6. The photograph of bubble generation at (**a**) MP and (**b**) MMN electrodes; (**c**) distribution of bubbles generated at each electrode.

The optical evaluation of the bubbles, as shown in Figure 6c, revealed that while the mesh electrodes in the pristine configuration produced a higher rate of fine bubbles (below 100 nm) compared to the plate electrodes, the overall bubble generation rate showed no significant difference between the two. However, applying micro-nano structures to the electrode surface resulted in a more than twofold increase in bubble generation compared to the pristine configuration, with a particularly high concentration of fine bubbles in the 100–150 nm range. Consequently, the MMN electrode design was identified as the most effective configuration for enhancing EF performance.

3.3. Evaluation of EF Performance for Micro-Nano Structured Mesh Electrode

EF is typically driven by the generation of gas bubbles at the electrode surface, which rise to the water surface. As they ascend, these bubbles collide with and agglomerate foreign matter in the liquid, leading to the flotation and separation of contaminants (Figure 7a). For a typical bubble with a diameter of 50 μm, the flotation velocity (V_{bubble}) is expressed using Equation (7) [56]:

$$V_{bubble} = \frac{2\left(\rho_{liquid} - \rho_{gas}\right)g}{9\eta} r^2 \quad (7)$$

where η is the viscosity constant of the liquid.

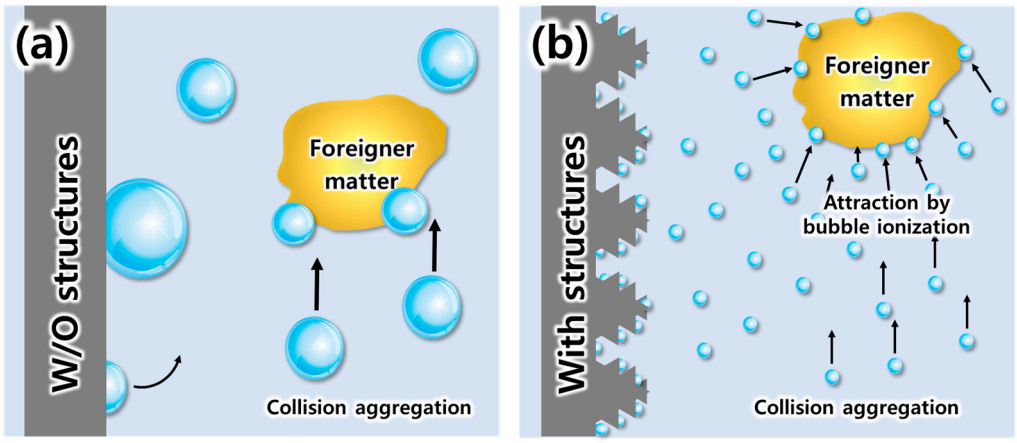

Figure 7. Schematic of EF process (**a**) without or (**b**) with micro-nano strucutured surface.

However, when bubbles are smaller than 50 μm in diameter, they begin to be influenced by Brownian motion. Brownian motion refers to the random movement of small particles suspended in a liquid, and the velocity (V_R) can be described using Equation (8) [57]:

$$V_R = \sqrt{\frac{3K_BT}{M}} \quad (8)$$

where K_B is the Boltzmann constant, T is the absolute temperature, and M is the mass of the particles.

As the bubble size approaches 50 μm or less, the flotation velocity and Brownian motion speed become comparable, causing the bubbles to ascend more slowly. For nanobubbles with a diameter below 1 μm, Brownian motion becomes dominant, resulting in extremely slow ascent. Moreover, these nanobubbles are stabilized by a layer of charged ions surrounding their surface, preventing rapid dissolution and allowing them to remain in the solution for extended periods [58,59].

This stability and prolonged presence of fine bubbles in the liquid offer distinct advantages for EF. In addition to the traditional collision-based agglomeration, fine bubbles benefit from Brownian motion-induced collisions and electrostatic interactions between the charged bubble surfaces and charged foreign particles. These effects significantly enhance the overall EF performance (Figure 7).

To verify this effect, EF tests were conducted using both the MP and MMN electrodes with a uniform oil-in-water mixture. The separation times were compared, and it was observed that the MP electrode required over 5 min to achieve phase separation, while the MMN electrode achieved the same result in approximately 30 s (Figure 8).

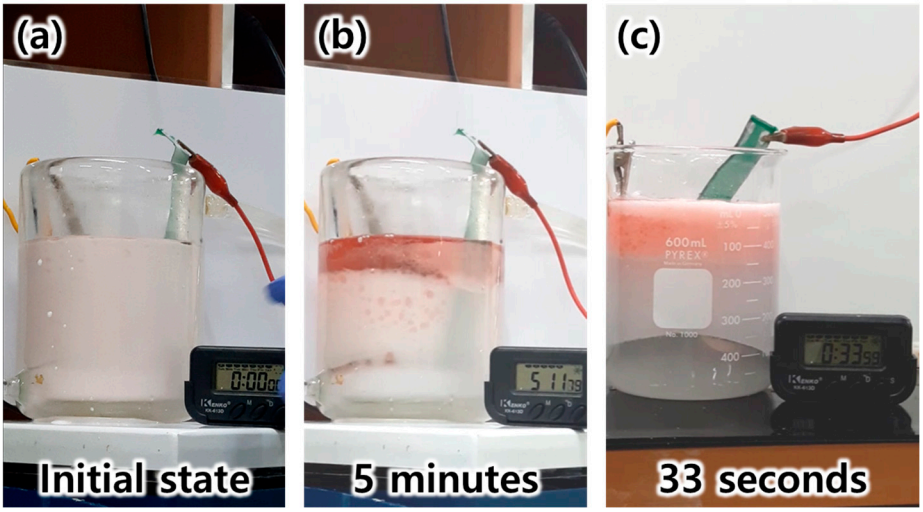

Figure 8. (**a**) Initial state of oil-in-water mixture and flotation time for (**b**) MP and (**c**) MMN.

To further assess the purification efficiency of the MMN electrode in EF, additional experiments were performed with various oil types, including n-dodecane, octane, petroleum ether, n-hexane, and toluene. The EF performance of the MMN electrode was compared to that of spontaneous flotation. As shown in Figure 2, after the flotation process, the residual oil concentrations in the solution were measured using Total Organic Carbon (TOC) analysis. The initial concentration of oil in the emulsion was approximately 80,000 mg/L. Figure 9 demonstrates that the EF performance using the micro-nano structured mesh electrode showed improvements ranging from a minimum of 52.5% for diesel to a maximum of 92.5% for hexane, compared to spontaneous flotation.

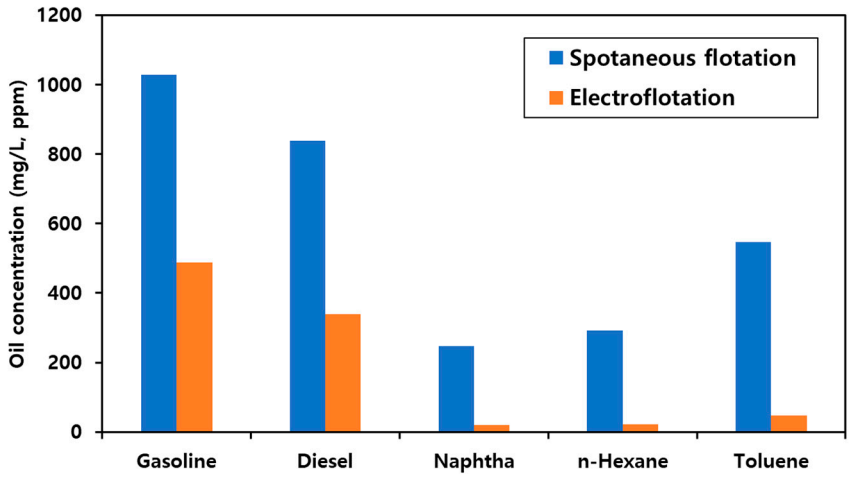

Figure 9. Comparison of residual oil concentrations for different oil types following 10 min of spontaneous and electroflotation.

4. Conclusions

In this study, we aimed to develop practical electrodes with improved durability and large-scale production capabilities by applying micro-nano structures to the electrode surface. To evaluate the enhanced performance, the electrochemical behavior of these electrodes was assessed using the EF process. Aluminum was selected as the optimal

material based on its superior bubble generation rate compared to titanium and copper. When micro-nano structures were applied to the aluminum electrodes, bubble generation significantly increased, while bubble size decreased, resulting in improved flotation performance. The MMN electrodes, in particular, produced over twice the number of bubbles as pristine electrodes, with a high concentration of fine bubbles in the 100–150 nm range. This increase in fine bubble production allowed the bubbles to remain in the solution longer, facilitating more interactions with oil droplets and contaminants. Compared to spontaneous flotation, the MMN electrodes demonstrated a much higher purification efficiency, reducing oil concentrations by up to 92.5% in the case of hexane.

This research not only optimized the EF process but also demonstrated that rapid bubble release from the micro-nano structured electrodes enhanced the overall reactivity of the electrodes. The ability to generate a higher volume of smaller bubbles is crucial for improving separation efficiency in EF, as it increases the likelihood of particle–bubble collisions, particularly with fine contaminants that are difficult to separate using traditional methods. Additionally, the extended retention time of nanobubbles in the solution further amplified the separation efficiency by promoting electrostatic interactions with charged contaminants.

The findings of this study provide valuable insights into the design and fabrication of high-performance electrodes for a wide range of applications. The enhanced EF performance demonstrated by the MMN electrodes underscores the potential for these electrodes to be utilized in industrial wastewater treatment and other systems requiring efficient separation processes. Overall, this work contributes to advancing electrode technology by showing how micro/nano structures can significantly improve both the electrochemical and flotation efficiencies of electrodes, paving the way for future research and practical implementations.

Supplementary Materials: The following supporting information can be downloaded at: https://www.mdpi.com/article/10.3390/app14219952/s1.

Author Contributions: Conceptualization, K.L. and M.K.; methodology, M.K.; validation, K.L., M.K., J.-H.P. and B.C.; formal analysis, K.L.; investigation, K.L., M.K. and. B.C.; resources, K.L. and W.H.; data curation, M.K.; writing—original draft preparation, K.L. and M.K.; writing—review and editing, K.L. and J.-H.P.; visualization, M.K.; supervision, W.H.; project administration, K.L.; funding acquisition, K.L. and J.-H.P. All authors have read and agreed to the published version of the manuscript.

Funding: This work was supported by a "Development of Hybrid Propulsion Ship 10 MW Class DC Distribution Technology" Program funded by the Ministry of Commerce Industry and Energy (1415188463/PNS5120). This research was also supported by a grant from "Development of technologies to improve passenger ship efficiency based on renewable energy (RS-2022-221551/PMS5960)" funded by the Ministry of Oceans and Fisheries of Korea. This research was also supported by a grant from the Endowment project of "Development of Basic Technologies in Eco-friendly Ship Fuel Reliability and Safety Evaluation" funded by Korea Research Institute of Ships and Ocean Engineering (2520000279/PES5100).

Institutional Review Board Statement: Not applicable.

Informed Consent Statement: Not applicable.

Data Availability Statement: The original contributions presented in the study are included in the article/Supplementary Material, further inquiries can be directed to the corresponding author.

Acknowledgments: The authors would like to express their sincere gratitude for the support provided by the Ministry of Commerce Industry and Energy, the Ministry of Oceans and Fisheries and Korea Research Institute of Ships and Ocean Engineering, Republic of Korea.

Conflicts of Interest: The authors declare no conflicts of interest.

References

1. Cecchini, R.; Pelosi, G. Alessandro Volta and his battery. *IEEE Antennas Propag. Mag.* **1992**, *34*, 30–37. [CrossRef] [PubMed]
2. Meng, J.; Guo, H.; Niu, C.; Zhao, Y.; Xu, L.; Li, Q.; Mai, L. Advances in structure and property optimizations of battery electrode materials. *Joule* **2017**, *1*, 522–547. [CrossRef]
3. Arthur, T.S.; Bates, D.J.; Cirigliano, N.; Johnson, D.C.; Malati, P.; Mosby, J.M.; Perre, E.; Rawls, M.T.; Prieto, A.L.; Dunn, B. Three-dimensional electrodes and battery architectures. *MRS Bull.* **2011**, *36*, 523–531. [CrossRef]
4. Yang, R.; Yao, W.; Tang, B.; Zhang, F.; Lei, X.; Lee, C.; Tang, Y. Development and challenges of electrode materials for rechargeable Mg batteries. *Energy Storage Mater.* **2021**, *42*, 687–704. [CrossRef]
5. Lee, Y.K. The effect of active material conductive additives and binder in a cathode composite electrode on battery performance. *Energies* **2019**, *12*, 658. [CrossRef]
6. Park, S.; Shi, B.; Shang, Y.; Deng, K.; Fu, K. Structured electrode additive manufacturing for lithium-ion batteries. *Nano Lett.* **2022**, *22*, 9462–9469. [CrossRef]
7. Kuang, Y.; Chen, C.; Kirsh, D.; Hu, L. Thick electrode batteries: Principles, opportunities, and challenge. *Adv. Energy Mater.* **2019**, *9*, 1901457. [CrossRef]
8. Su, Y.; Fu, Y.; Wei, Y.; Yan, J.; Mao, B. The electrode/ionic liquid interface: Electric double layer and metal electrodeposition. *ChemPhysChem* **2010**, *11*, 2764–2778. [CrossRef]
9. Yan, Z.; Liu, H.; Hao, Z.; Yu, M.; Chen, X.; Chen, J. Electrodeposition of (hydro)oxides for an oxygen evolution electrode. *Chem. Sci.* **2020**, *11*, 10614–10625. [CrossRef]
10. Hao, F.; Verma, A.; Mukherjee, P.P. Electrodeposition stability of metal electrodes. *Energy Storage Mater.* **2019**, *20*, 1–6. [CrossRef]
11. Litser, S.; McLean, G. PEM fuel cell electrodes. *J. Power Sources* **2004**, *130*, 61–76. [CrossRef]
12. Kundu, S.; Fowler, M.W.; Simon, L.C.; Grot, S. Morphological features (defects) in fuel cell membrane electrode assemblies. *J. Power Sources* **2006**, *157*, 650–656. [CrossRef]
13. Chen, D.; Pei, P.; Li, Y.; Ren, P.; Meng, Y.; Song, X.; Wu, Z. Proton exchange membrane fuel cell stack consistency: Evaluation methods, influencing factors, membrane electrode assembly parameters and improvement measures. *Energy Convers. Manag.* **2022**, *261*, 115651. [CrossRef]
14. Wang, Y.; Zhang, L.; Hou, H.; Xu, W.; Duan, G.; He, S.; Liu, K.; Jiang, S. Recent progress in carbon-based materials for supercapacitor electrodes: A review. *J. Mater. Sci.* **2021**, *56*, 173–200. [CrossRef]
15. Xu, B.; Zhang, H.; Mei, H.; Sun, D. Recent progress in metal-organic framework-based supercapacitor electrode materials. *Coord. Chem. Rev.* **2020**, *420*, 213438. [CrossRef]
16. Yue, T.; Shen, B.; Gao, P. Carbon material/MnO_2 as conductive skeleton for supercapacitor electrode material: A review. *Renew. Sustain. Energy Rev.* **2022**, *158*, 112131. [CrossRef]
17. Wan, L.; Xu, Z.; Xu, Q.; Pang, M.; Lin, D.; Liu, J.; Wang, B. Key components and design strategy of the membrane electrode assembly for alkaline water electrolysis. *Energy Environ. Sci.* **2023**, *16*, 1384. [CrossRef]
18. Mayerhofer, B.; McLaughlin, D.; Bohm, T.; Hegelheimer, M.; Seeberger, D.; Thiele, S. Bipolar membrane electrode assemblies for water electrolysis. *ACS Appl. Energy Mater.* **2020**, *3*, 9635–9644. [CrossRef]
19. Liang, S.; Jiang, M.; Lun, H.; Ma, Y.; Yang, J. A high-rate electrode with grotthuss topochemistry for membrane-free decoupled acid water electrolysis. *Adv. Energy Mater.* **2021**, *11*, 2102057. [CrossRef]
20. Zhang, Z.; Lees, E.W.; Habibzadeh, F.; Salvatore, D.A.; Ren, S.; Simpson, G.L.; Wheeler, D.G.; Liu, A.; Berlinguette, C.P. Porous metal electrodes enable efficient electrolysis of carbon capture solutions. *Enegry Environ. Sci.* **2022**, *15*, 705–713. [CrossRef]
21. Mockl, M.; Ernst, M.F.; Kornherr, M.; Allebrod, F.; Bernt, M.; Byrknes, J.; Eickes, C.; Gebauer, C.; Moskovteseva, A.; Gasteiger, H.A. Durability testing of low-iridium PEM water electrolysis membrane electrode assemblies. *J. Electrochem. Soc.* **2022**, *169*, 064505. [CrossRef]
22. Wang, S.; Lu, A.; Zhong, C. Hydrogen production from water electrolysis: Role of catalysts. *Nano Converg.* **2021**, *8*, 4. [CrossRef] [PubMed]
23. Li, R.; Li, Y.; Yang, P.; Wang, D.; Xu, H.; Wang, B.; Meng, F.; Zhang, J.; An, M. Electrodeposition: Synthesis of advanced transition metal-based catalyst for hydrogen production via electrolysis of water. *J. Energy Chem.* **2021**, *57*, 547–566. [CrossRef]
24. Zhou, B.; Gao, R.; Zou, J.; Yang, H. Surface design strategy of catalysts for water electrolysis. *Small* **2022**, *18*, 2202336. [CrossRef] [PubMed]
25. Khan, A.A. Electrode wear and material removal rate during EDM of aluminum and mild steel using copper and brass electrodes. *Int. J. Adv. Manuf. Technol.* **2008**, *39*, 482–487. [CrossRef]
26. Ran, Q.; Shi, H.; Meng, H.; Zeng, S.P.; Wan, W.B.; Zhang, W.; Wen, Z.; Lang, X.Y.; Jiang, Q. Aluminum-copper alloy anode materials for high-energy aqueous aluminum batteries. *Nat. Commun.* **2022**, *13*, 576. [CrossRef]
27. Dhanabalan, S.; Sivakumar, K.; Narayanan, C.S. Experimental investigation on electrical discharge machining of titanium alloy using copper, brass and aluminum electrodes. *J. Eng. Sci. Technol.* **2015**, *10*, 72–80.
28. Su, H.; Wu, D.; Li, C.; Li, C.; Zhang, C. Research advances on electrode materials for solid oxide electrolysis cells. *Prog. Nat. Sci. Mater. Int.* **2023**, *33*, 309–319. [CrossRef]
29. Hughes, J.P.; Clipsham, J.; Chavushoglu, H.; Rowley-Neale, S.J.; Banks, C.E. Polymer electrolyte electrolysis: A review of the activity and stability of non-precious metal hydrogen evolution reaction and oxygen evolution reaction catalysts. *Renew. Sustain. Energy Rev.* **2021**, *139*, 110709. [CrossRef]

30. Khouya, A. Hydrogen production costs of a polymer electrolyte membrane electrolysis powered by a renewable hybrid system. *Int. J. Hydrogen Energy* **2021**, *46*, 14005–14023. [CrossRef]
31. Zhang, F.; Zhang, H.; Salla, M.; Qin, N.; Gao, M.; Ji, Y.; Huang, S.; Wu, S.; Zhang, R.; Lu, Z.; et al. Decoupled redox catalytic hydrogen production with a robust electrolyte-borne electron and proton carrier. *J. Am. Chem. Soc.* **2020**, *143*, 223–231. [CrossRef] [PubMed]
32. Ulleberg, Ø. Modeling of advanced alkaline electrolyzers: A system simulation approach. *Int. J. Hydrogen Energy* **2003**, *28*, 21–33. [CrossRef]
33. Chen, M.; Chou, S.F.; Blaabjerg, F.; Davari, P. Overview of power electronic converter topologies enabling large-scale hydrogen production via water electrolysis. *Appl. Sci.* **2022**, *12*, 1906. [CrossRef]
34. Kojima, H.; Nagasawa, K.; Todoroki, N.; Ito, Y.; Matsui, T.; Nakajima, R. Influence of renewable energy power fluctuations on water electrolysis for green hydrogen production. *Int. J. Hydrogen Energy* **2023**, *48*, 4572–4593. [CrossRef]
35. Shen, J.; Li, J.; Li, B.; Zheng, Y.; Bao, X.; Guo, J.; Guo, Y.; Lai, C.; Lei, W.; Wang, S.; et al. Ambient fast synthesis of super-aerophobic/superhydrophilic electrode for superior electrocatalytic water oxidation. *Energy Environ. Mater.* **2023**, *6*, e12462. [CrossRef]
36. Andaveh, R.; Darband, G.B.; Maleki, M.; Rouhaghdam, A.S. Superaerophobic/superhydrophilic surfaces as advanced electrocatalysts for the hydrogen evolution reaction: A comprehensive review. *J. Mater. Chem. A* **2022**, *10*, 5147–5173. [CrossRef]
37. Kim, Y.; Lee, S.; Cho, H.; Park, B.; Kim, D.; Hwang, W. Robust superhydrophilic/hydrophobic surface based on self-aggregated Al_2O_3 nanowires by single-step anodization and self-assembly method. *ACS Appl. Mater. Interfaces* **2012**, *4*, 5074–5078. [CrossRef]
38. Cho, H.; Kim, D.; Lee, C.; Hwang, W. A simple fabrication method for mechanically robust superhydrophobic surface by hierarchical aluminum hydroxide structures. *Curr. Appl. Phys.* **2013**, *13*, 762–767. [CrossRef]
39. Kwak, W.; Hwang, W. Facile method for preparing superoleophobic surfaces with hierarchical microcubic/nanowire structures. *Nanotechnology* **2015**, *27*, 055301. [CrossRef]
40. Tiringer, U.; Van Dam, J.P.B.; Abrahami, S.T.; Terryn, H.; Kovač, J.; Milošev, I.; Mol, J.M.C. Scrutinizing the importance of surface chemistry versus surface roughness for aluminium/sol-gel film adhesion. *Surf. Interfaces* **2021**, *26*, 101417. [CrossRef]
41. Lee, K.; Hwang, W.; Cho, H. Development of a versatile coating based on hydrolysis-assisted self-bonding and structure evolution of aluminum nitride nanopowder: Application toward repairing severe damages on superhydrophobic surfaces. *Surf. Coat. Technol.* **2023**, *460*, 129431. [CrossRef]
42. Adetunji, A.I.; Olaniran, A.O. Treatment of industrial oily wastewater by advanced technologies: A review. *Appl. Water Sci.* **2021**, *11*, 98. [CrossRef]
43. Chen, G. Electrochemical technologies in wastewater treatment. *Sep. Purif. Technol.* **2004**, *38*, 11–41. [CrossRef]
44. Almeida, C.C.D.; Costa, P.R.F.D.; Melo, M.J.D.M.; Santos, E.V.D.; Martínez-Huitle, C.A. Application of electrochemical technology for water treatment of Brazilian industry effluents. *J. Mex. Chem. Soc.* **2014**, *58*, 276–286.
45. Hacha, R.R.; Merma, A.G.; Couto, H.J.B.; Torem, M.L. Measurement and analysis of H2 and O2 bubbles diameter produced by electroflotation processes in a modified Partridge-Smith cell. *Powder Technol.* **2019**, *342*, 308–320. [CrossRef]
46. Santos, G.D.O.S.; de Salles Pupo, M.M.; Vasconcelos, V.M.; Eguiluz, K.I.B.; Banda, G.R.S. Electroflotation. In *Electrochemical Water and Wastewater Treatment*; Butterworth-Heinemann: Oxford, UK, 2018; pp. 77–118.
47. Kyzas, G.Z.; Matis, K.A. Electroflotation process: A review. *J. Mol. Liq.* **2016**, *220*, 657–664. [CrossRef]
48. Moussa, D.T.; El-Nass, M.H.; Nasser, M.; Al-Marri, M.J. A comprehensive review of electrocoagulation for water treatment: Potential and challenges. *J. Environ. Manag.* **2017**, *186*, 24–41. [CrossRef]
49. Vespsalainen, M.; Sillanpaa, M. Electrocoagulation in the treatment of industrial waters and wastewaters. In *Advanced Water Treatment*; Sillanpaa, M., Ed.; Elsevier: Amsterdam, The Netherlands, 2020; pp. 1–78.
50. Mouedhen, G.; Feki, M.; Wery, M.D.P.; Ayedi, H.F. Behavior of aluminum electrodes in electrocoagulation process. *J. Hazard. Mater.* **2008**, *150*, 124–135. [CrossRef]
51. Gurney, R.W. The quantum mechanics of electrolysis. *Contain. Pap. Math. Phys. Character* **1931**, *134*, 137–154.
52. Liger-Belair, G.; Marchal, R.; Robillard, B.; Vignes-Adler, M.; Maujean, A.; Jeandet, P. Study of effervescence in a glass of champagne: Frequencies of bubble formation, growth rates, and velocities of rising bubbles. *Am. J. Enol. Vitic.* **1999**, *50*, 317–323. [CrossRef]
53. Aune, R.; Battezzati, L.; Brooks, R.; Egry, I.; Fecht, H.J.; Garandet, J.P.; Mills, K.C.; Passerone, A.; Quested, P.N.; Ricci, E.; et al. Surface tension and viscosity of industrial alloys from parabolic flight experiments—Results of the ThermoLab project. *Microgravity-Sci. Technol.* **2005**, *16*, 11–14. [CrossRef]
54. Brillo, J.; Egry, I. Surface tension of nickel, copper, iron and their binary alloys. *J. Mater. Sci.* **2005**, *40*, 2213–2216. [CrossRef]
55. Bainbridge, I.F.; Taylor, J.A. The surface tension of pure aluminum and aluminum alloys. *Metall. Mater. Trans. A* **2013**, *44*, 3901–3909. [CrossRef]
56. Bian, H.; Kurwitz, C.; Sun, Z.; Cheng, K.; Chen, K. Enhanced nucleate boiling on 3D-printed micro-porous structured surface. *Appl. Therm. Eng.* **2018**, *141*, 422–434. [CrossRef]
57. Landau, L.D.; Akhierzer, A.I.; Lifshitz, E.M. Heat. In *General Physics: Mechanics and Molecular Physics*, 1st ed.; Pergamon Press: Oxford, UK, 1967; pp. 144–149.

58. Yoon, R.H.; Yordan, J.L. Zeta-potential measurements on microbubbles generated using various surfactants. *J. Colloid Interface Sci.* **1986**, *113*, 430–438. [CrossRef]
59. Agarwal, A.; Ng, W.J.; Liu, Y. Principle and applications of microbubble and nanobubble technology for water treatment. *Chemosphere* **2011**, *84*, 1175–1180. [CrossRef]

Disclaimer/Publisher's Note: The statements, opinions and data contained in all publications are solely those of the individual author(s) and contributor(s) and not of MDPI and/or the editor(s). MDPI and/or the editor(s) disclaim responsibility for any injury to people or property resulting from any ideas, methods, instructions or products referred to in the content.